Clinical Implementation of Deep Learning MR reconstruction for TSE Sequences: Reduction of Acquisition Time and Maintenance

Judith Herrmann
Universitätsklinikum Tübingen
Sebastian Gassenmaier
Universitätsklinikum Tübingen
Thomas Kuestner
Universitätsklinikum Tübingen
Matthias Kuendel
Universitätsklinikum Tübingen
Dominik Nickel
Siemens Healthcare (Germany)
Gregor Koerzdoerfer
Siemens Healthcare (Germany)
Mahmoud Mostapha
Siemens (United States)
Mariappan Nadar
Siemens (United States)
Ahmed Othman (ahmed.e.othman@googlemail.com)
Universitätsklinikum Tübingen

Research Article

Keywords: Magnetic Resonance Imaging, Deep Learning Reconstruction, Image Processing, Diagnostic Imaging.

Posted Date: February 3rd, 2021

DOI: https://doi.org/10.21203/rs.3.rs-153369/v1

Abstract

Background:

The application of Deep Learning (DL) in MR image reconstruction is increasingly gaining attention due to its potential of increasing image quality and reducing acquisition time. However, the technology hasn't been yet implemented in clinical routine. The aim of this study was therefore to describe the implementation of this novel DL image reconstruction for turbo spin echo (TSE) sequences in clinical workflow including a thorough explanation of the required steps and an evaluation of the obtainable image quality compared to conventional TSE.

Methods:

DL image reconstruction using a variational network was clinically implemented to enable acquisition of accelerated TSE sequences. After internal review board's approval and informed consent, 30 examinations for knee, shoulder, and lumbar spine in 15 volunteers at 3 T were included in this prospective study. Conventional TSE sequences (TSE) and TSE with deep learning reconstruction (TSE_{DL}) were compared regarding overall image quality, noise, sharpness, and subjective signal-to-noise-ratio (SNR), as well diagnostic confidence and image impression. Comparative analyses were conducted to assess the differences between the sequences. A survey on technologists' acceptance was performed for DL image reconstruction.

Results:

DL image reconstruction was successfully implemented in a clinical workflow and TSE_{DL} allowed a remarkable time saving of more than 50%. Overall image quality, diagnostic confidence and image impression for TSE_{DL} were rated as excellent (median 4, IQR 4-4) and comparable to TSE (image quality: $p=0.059$, diagnostic confidence: $p=0.157$, image impression: $p=0.102$). Noise, sharpness, artifacts, and subjective SNR for TSE_{DL} reached significantly superior levels to TSE (noise: $p<0.001$, sharpness: $p=0.001$, artifacts: $p=0.014$, subjective SNR: $p<0.001$). Technologists reported high levels of acceptance for DL image reconstruction. Required time for the reconstruction process was rated moderate and longer than standard sequences (median 2, IQR 2-3). Required time and effort for the implementation in daily workflow was rated as low effort (median 4, IQR 3-4). General applicability of DL reconstruction as well as acceptance of DL sequences in clinical routine were rated excellent (median 4, IQR 3-4).

Conclusion:

DL image reconstruction for TSE sequences can be implemented in clinical workflow and enables a remarkable time saving (>50%) in image acquisition while maintaining excellent image quality.

Trial registration:

Your clinical trial is officially registered at the German DRKS with the registration number: **DRKS00023278.**

Introduction

Magnetic Resonance Imaging (MRI) has become a modality of choice for the diagnosis of several diseases and is currently indispensable in healthcare. One big disadvantage of MRI is the long examination duration, which are not tolerated by a substantial proportion of patients and, on the other hand, come along with other downsides such as decreased image quality due to motion artifacts, increased costs and reduced patient throughput (1).

The acquisition time of MRI is primarily determined by the achievable sampling rate for a given contrast and image quality which in turn is determined by the number of samples needed for the image reconstruction for a given size and resolution. Over the past decades, different acceleration strategies have been proposed and established such as parallel imaging (PI) and Compressed Sensing (CS). These techniques acquire reduced k-space data with an array of receiver coils and afterwards reconstruct images from the acquired, undersampled data (2, 3). Artifacts due to residual aliasing, or stair casing and blurring can impair achievable image quality of those acceleration strategies.

Recently, a new acceleration strategy gained attention: Deep Learning (DL) reconstruction, as discussed here and detailed below, may solve non-linear and ill-posed reconstruction problems efficiently (4–6). Instead of *ad hoc* regularization that enforces sparsity, the regularization is trained on representative images. This procedure also allows the regularization to generalize for different sampling patterns, acceleration factors, and artifact behavior. Most prominently, the DL networks are trained in a supervised manner, i.e. representative fully sampled data with known results for the given application – so called ground truth data - are available which allow retrospective subsampling and training of the architectures. Testing is performed on a separate set of samples (not seen in training) with subsampled datasets. Realistic performance assessment should be performed on prospectively subsampled datasets. While training can be computationally intensive and takes rather long, it can be performed offline. The trained architecture can then be used in testing to reconstruct an aliasing and noise-free image within a few seconds and with greatly reduced computational demand.

DL reconstruction has been recently shown to potentially accelerate image acquisition in knee MRI (7), however, the majority of existing literature on this topic focusses on offline solutions simulating accelerated image acquisition. The evaluation of the clinical value of DL reconstruction requires an implementation in clinical settings and a prospective acquisition of accelerated data.

Therefore, the aim of this report is to describe the implementation of DL image reconstruction in clinical workflow including a thorough explanation of the required steps in patient care and an evaluation of the obtainable image quality for accelerated DL-based TSE sequences (TSE_{DL}) in comparison to conventional TSE sequences (TSE).

Materials And Methods

Institutional review board approval was obtained for this prospective, monocentric study. All study procedures were conducted in accordance with the ethical standards as laid down in the 1964 Declaration of Helsinki and its later amendments.

Acceleration strategies for DL accelerated MRI

With DL reconstruction providing higher signal-to-noise ratio (SNR) and allowing for higher acceleration with conventional sampling patterns, the data acquisition can be tailored.

For TSE acquisitions modifying the original acquisition's image contrast is usually not a desirable goal for tailored acquisitions. Rather, DL reconstruction in MRI can be used to improve on a combination of image resolution, acquisition time, and SNR while maintaining the original contrast.

In contrast to that, some applications like the Half-Fourier single-shot turbo spin echo (HASTE) sequence provide fast and robust acquisitions at the cost of image contrast as compared to the TSE sequence. Here, the improved DL reconstruction enables acquisition protocols providing improved image contrast. Specifically, with a higher acceleration factor the duration of the echo train can be shortened, and therefore, the effect of T2 decay can be reduced. As an additional benefit, the specific absorption rate (SAR) is reduced with the number of required refocusing pulses. This allows for further sequence optimizations in the form of larger gaps between consecutively acquired slices and reduced repetition times.

Besides the data acquisition for the actual image data, calibration data for the coil-sensitivity estimation needs to be acquired. For the TSE sequence, these data which cover the center of k-space (typically about 16 phase-encoding lines) are acquired as part of the imaging scan.

A conventional under-sampling pattern as known from parallel imaging is used. As shown in earlier works (8, 9), these provide the same performance when reconstructed with DL-based methods as incoherent sampling patterns favored by CS. They have the important advantages of being clinically established and are highly flexible regarding adaptations of resolution and signal evolution during sampling. Furthermore, their artifact behavior with regard to motion, reduced field-of-view, and aliasing is well-known and potentially even improved by the DL-based reconstruction. Also, as a part of conventional under-sampling patterns, a fraction of the k-space's periphery is often not acquired in order to reduce acquisition time. This effectively reduces the resolution in the phase-encoding direction and is referred to as phase resolution. It describes the fraction of acquired data in the phase-encoding direction in percent neglecting the regular parallel imaging type of under-sampling. For illustration, an exemplary sampling pattern of acceleration factor 2 and a phase resolution < 100% is shown in **Figure 1**. A calibration region around the k-space center is fully sampled and used for the estimation of coil-sensitivity maps.

Deep Learning Image Reconstruction

For all discussed applications, the prototype image reconstruction comprises a fixed iterative reconstruction scheme or variational network (9, 10). The fixed unrolled algorithm for accelerated MR image reconstruction consists of multiple cascades, each made up from a data consistency using a trainable Nesterov Momentum followed by a CNN-based regularization. The regularization model's architecture is based on a novel hierarchical design of an iterative network that repeatedly decreases and increases the resolution of the feature maps, allowing for a more memory-efficient model than conventional CNNs. In addition to the input under-sampled k-space data, coil-sensitivity maps are also provided, which are estimated from the calibration data as a pre-processing step. Also, a bias-field is extracted from a separate adjustment acquisition for image homogenization. The architecture of the reconstruction network is illustrated in **Figure 2**. During the training phase, the bias-field is inserted into the image reconstruction as a final correction step.

For the image reconstruction k-space data, bias-field correction and coil-sensitivity maps are inserted into the variational network. Compared to previous works and the previously described cascades, the variational network also utilizes two additional types of cascades, namely, pre- and post-cascades. Like regular cascades, pre-cascades employ trainable extrapolation; however, no regularization is applied, allowing the network to focus on parallel imaging. Such design is motivated by the empirical finding that initial steps in the variational network focus on the signal recovery of missing data near the k-space center. This approach supports acquisitions without integrated calibration and flexible k-space sampling. Finally, post-cascades employing non-trainable extrapolation are also utilized for further guarantees on the data consistency, which minimizes the risk of hallucination when adversarial training is applied. The network is first trained to minimize the combined L1 and a multi-scale version of the structural similarity (SSIM) content losses between network prediction and ground truth images. A semi-supervised refinement is applied in a subsequent training step where an adversarial loss based on Wasserstein Generative Adversarial Networks (WGAN) is also added (11).

The reconstruction was trained on volunteer acquisitions using conventional TSE protocols. About 10,000 slices were acquired on volunteers using clinical 1.5T and 3T scanners (MAGNETOM scanners, Siemens Healthcare, Erlangen, Germany). Fully sampled acquisitions with high resolution were performed in head, pelvis, and knee using representative contrasts for the respective body regions. The training data therefore included a wide range of image contrasts, orientations, body regions, and resolutions. For both sequence types, the input to the reconstruction network was retrospectively down-sampled to an acceleration factor of 4. The training was implemented in PyTorch and performed on a GPU cluster NVIDIA Tesla V100 (32GB of memory) GPU.

Implementation of DL image reconstruction in clinical workflow

For deployment in the scanner reconstruction pipeline, the obtained network was converted to a C++ implemented inference framework. For the CPU-only reconstruction on a clinical MRI scanner, inference needed about 2 seconds per slice for the used protocol settings. The reconstruction was triggered after the end of the acquisition, which resulted in a perceived reconstruction time of 2-3 minutes including

additional pre- and post-processing. GPU-based reconstruction brings the duration down to the order of 10 seconds for a complete dataset but was not available in the local setting of this study.

Diagnostic image evaluation

Accelerated TSE_{DL} sequences were prospectively acquired along with standard TSE sequences at clinical 3T MRI scanner (MAGNETOM, Siemens Healthcare, Erlangen, Germany), and a final sample of 30 examinations in 15 volunteers were included in this analysis, see **Table 1**.

TABLE 1. Demographics of included individuals	
Variables	
Total (male/female), n	30 (20/10)
	knee: 10 (7/3)
	shoulder: 10 (6/4)
	lumbar spine: 10 (7/3)
Age, mean ± SD (range), y	total: 28 ± 7 (20 - 54)
	knee: 27 ± 4 (20 - 31)
	shoulder: 30 ± 10 (20 – 54)
	lumbar spine: 28+7 (20 – 43)
SD indicates standard deviation; y, years; n, number.	

Two radiologists with 9 years and 3 years of experience in MRI independently rated both TSE and TSE_{DL} by using a random order.

Overall image quality, artifacts, noise, sharpness, subjective SNR, as well as diagnostic confidence and image impression ratings were performed on an ordinal 4-point Likert scale (1 = non-diagnostic, with major streak artifacts; 2 = non-diagnostic, moderate artifacts with low image quality; 3 = minor artifacts with good image quality; 4 = no artifacts with excellent image quality; image impression: 1 = very unrealistic, 2 = unrealistic, 3 = realistic, and 4 = very realistic). Reading scores were considered sufficient when reaching ≥ 3.

Image analysis was performed on a PACS workstation (GE Healthcare Centricity™ PACS RA1000, Milwaukee, WI, USA).

Statistical analyses were performed using SPSS version 26 (IBM Corp, Armonk, NY, USA). Besides descriptive statistics, compromising median and interquartile range (IQR), the reading score of the

qualitative image analysis of the TSE sequences were compared using a paired Wilcoxon signed-rank test. Significance was assumed at a level of $P < 0.05$.

Inter-rater agreement was calculated through Cohen's kappa. Kappa values were interpreted as follows: 0–0.20 = poor agreement, 0.21–0.40 = fair agreement, 0.41–0.60 = moderate agreement, 0.61–0.80 = substantial agreement, 0.81–1 = (almost) perfect agreement.

Technologists' assessment

Five MRI technologists were included in this survey. On a 4-point Likert scale, the required time for reconstruction process (1 = long reconstruction time, 2 = moderate, 3 = low, 4 = very low reconstruction time), the required time and effort for implementation in workflow (1 = high, 2 = moderate, 3 = low, 4 = very low), as well as the technical stability (1 = low technical stability, 2 = moderate technical stability, 3 = good technical stability, 4 = excellent technical stability), and acceptance of DL sequences in clinical workflow (1 = low acceptance, 2 = moderate acceptance, 3 = good acceptance 4 = high acceptance) was evaluated.

Results

Implementation of DL image reconstruction in clinical workflow

The aim was to implement DL image reconstruction for TSE sequences in clinical workflow. All TSE_{DL} were successfully implemented in clinical workflow and were successfully acquired in all for all body parts. Fat suppression could be applied successfully for the implemented TSE_{DL}. TSE_{DL} allowed a remarkable time saving of more than 50% for each sequence, for instance T1-weighted TSE in sagittal orientation for lumbar spine required an acquisition time of 2:45 minutes compared to T1-weighted TSE_{DL} with an acquisition time of 58 seconds.

Table 2
Acquisition parameters of TSE and TSEDL at 3 T

Body Part	Shoulder		Knee		Lumbar spine	
	standard	DL	standard	DL	standard	DL
Sequence	TSE PD fs	TSE PD fs	TSE PD fs	TSE PD fs	T1 TSE	T1 TSE
Orientation	axial	axial	coronal	coronal	sagittal	sagittal
TA, min	2:14	1:10	3:11	1.33	2:45	0:58
FOV, mm	180	180	150	150	300	300
Voxel Size, mm	0.6 x 0.6 x 3.0	0.6 x 0.6 x 3.0	0.2 x 0.2 x 3.0	0.5 x 0.5 x 3.0	0.7 x 0.7 x 3.0	0.7 x 0.7 x 3.0
Averages	1	1	2	1	1	1
Concatenations	2	1	1	1	2	2
PAT	2	3	3	3	3	2
TR, ms	3000	3520	3790	3580	562	462
TE, ms	44	44	44	41	10	10
FA, degree	150	150	150	150	150	150
Bandwith, Hz/Px	180	180	100	120	180	180
Echo spacing, ms	10.9	10.9	14.6	13.7	10.4	10.4

TA indicates time of acquisition; FOV, field of view; PAT, Parallel Acquisition Technique; TE/TR, echo time/repetition time; FA, flip angle; TSE, turbo spin echo; PD, Proton Densitiy; FS, fat saturation.

An overview of exemplary acquisition parameters is displayed in Table 2.

Diagnostic image evaluation

Overall IQ was rated excellent for TSE_{DL} (median 4, IQR 4-4), comparable to TSE (P = 0.059). Image examples are shown in **Figures 3-5**.

Noise, sharpness, artifacts, subjective SNR were also rated excellent for TSE_{DL} (noise: median 4, IQR 4-4; sharpness: median 4, IQR 4-4; artifacts: median 4, IQR 3-4; subjective SNR: median 4, IQR 4-4) and significantly higher compared to TSE (noise: median 3, IQR 3-4, $p < 0.001$; sharpness: median 4, IQR 3-4, $p = 0.001$; artifacts: median 4, IQR 3-4, $p = 0.014$; subjective SNR: median 3, IQR 3-4, $p < 0.001$). No significant differences were found between the sequences concerning diagnostic confidence and image impression as both were rated excellent (TSE_{DL}: median 4, IQR 4-4; TSE: median 4, IQR 4-4; diagnostic confidence: $p = 0.157$, image impression: $p = 0.102$).

An overview of all results is displayed in **Table 3**.

TABLE 3. Image Quality, Inter-reader Agreement and Comparison of TSE and TSE_{DL}

	TSE_{DL}			TSE			TSE vs TSE_{DL}	
	R1	R2	κ	R1	R2	κ	R1	R2
	m (IQR)	m (IQR)		m (IQR)	m (IQR)			
$IQ_{overall}$	4 (4-4)	4 (4-4)	0.839	4 (3-4)	4 (3-4)	0.754	0.059	0.059
IQ_{noise}	4 (4-4)	4 (4-4)	0.651	3 (3-4)	3 (3-3)	0.703	<0.001	<0.001
$IQ_{sharpness}$	4 (4-4)	4 (4-4)	0.651	4 (3-4)	3 (3-4)	0.571	0.001	<0.001
$IQ_{artifacts}$	4 (3-4)	4 (4-4)	0.737	4 (3-4)	4 (3-4)	0.675	0.014	0.005
IQ_{sSNR}	4 (4-4)	4 (4-4)	0.651	3 (3-4)	3 (3-4)	0.610	<0.001	<0.001
IQ_{DC}	4 (4-4)	4 (4-4)	0.651	4 (4-4)	4 (4-4)	0.630	0.157	0.564
IQ_{II}	4 (4-4)	4 (4-4)	0.792	4 (4-4)	4 (4-4)	0.783	0.102	0.257

IQ indicates Image Quality; II, image impression; sSNR, subjective SNR; DC, Diagnostic Confidence; R, Reader; m, median; κ, Cohen's κ (Inter-rater Reliability); IQR, Interquartile Range.

Questionnaire for technologists

Required time for the reconstruction process was rated moderate and slower than standard sequences (median 2, IQR 2-3). Required time and effort for the implementation in daily workflow was rated as low effort (median 4, IQR 3-4). Technical performance as well as acceptance of DL sequences in daily routine were rated excellent (median 4, IQR 3-4).

Discussion

The aim of this report was to describe the implementation of DL image reconstruction in clinical workflow and to evaluate the obtainable image quality for TSE sequences. DL image reconstruction could be easily implemented in clinical routine in our institution with high acceptance among technologists.

TSE_{DL} provided excellent overall image quality and diagnostic confidence and is comparable to conventional TSE. Moreover, concerning noise, sharpness, artifacts, subjective SNR TSE_{DL} was rated significantly higher compared to TSE. DL-based reconstructions produce images that can exhibit even lower noise levels than a corresponding fully sampled conventional acquisition and may therefore look artificial to experienced radiologists.

Nonetheless, image impression was rated as excellent for both sequences.

Another aim of the study was to accelerate TSE sequence acquisition by the incorporation of DL image reconstruction. DL allowed for an acquisition time reduction of ≥50% while maintaining excellent image quality and diagnostic confidence. DL seems therefore to allow for higher accelerations than prior accelerations techniques.

Prior to DL image reconstruction, high acceleration levels beyond the Nyquist-Shannon sampling limit could be obtained by CS. In fact, if images can be sparsely represented in some transform domain, then a random and incoherent sub-Nyquist sampling together with an appropriate non-linear iterative image reconstruction allows aliasing-free recovery from incompletely sampled k-space data (2). CS employs iterative reconstruction algorithms that use *a priori* fixed sparsity-promoting transformation. Furthermore, the *a priori* assumption on sparsity with application-specific regularization weighting can, if not chosen appropriately, result in residual aliasing (under-regularized) or stair casing and blurring (over-regularized). Depending on the imaging application and sequence, a sampling trajectory that follows a desired random distribution can be challenging to implement without introducing other artifacts, e.g. by eddy currents due to strong switching gradients. Overall, these factors can impair achievable image quality and/or limit the achievable acceleration. The implementation of DL can overcome this drawback, and enables the acceleration of MR acquisition without impairing image quality.

Current Deep Learning-based image reconstruction uses super-vised learning techniques with convolutional neural networks (CNNs) (8, 12). DL networks have been proposed that operate on parallel imaging (PI)–accelerated acquisitions (9, 10, 13) and on CS-accelerated acquisitions (14). Proposed methods primarily differ in the way the DL network is applied in the image reconstruction and how data consistency is enforced between reconstructed images and acquired data: i) the network acts as trainable denoiser without explicit data consistency inside the architecture during training, but handling it in outer optimization schemes (plug-and-play denoisers), ii) physics-based reconstructions that incorporate data consistency during training. Networks furthermore differ in the chosen architectures (VN, UNet, cascaded CNN, etc.), raw k-space or noisy/aliased image input, the input dimensionality (2D, 3D, 2D + time, 3D + time, etc.), single- or multi-parametric input, complex- or real-valued processing of the complex-valued data, and single-coil (coil-combined) or multi-coil processing (9, 10, 14–26). To date, there are only a small number of published studies using DL methods on k-space data for MR image reconstruction in a clinical setting. Although the results are promising, routine application in clinical practice remains rare. As we successfully implemented DL reconstruction in imaging of different body regions, this report is intended to motivate radiologists to establish new AI techniques in everyday clinical practice to further accelerate MR imaging and gain access to MRI for more patients. Prolonged scanning duration can cause patient inconvenience and also limits the availability of MRI, what makes the single examination slots expansive. Drastic acceleration and cut-down of examination times might display one piece of the big puzzle to enhance healthcare and balance the weight of supply and demand. One of the most challenging tasks in medicine has always been finding a compromise between best medical care and best economical outcome. As most healthcare systems worldwide are insurance based using different

architectures (mandatory versus voluntary; public health insurance versus private sector), all systems face the same problem: shortage of money versus increased demand due to development of new expensive therapies, increase in expectancy of life, and new diagnostic possibilities. Reduction of TA might allow for a higher number of examinations per day.

This report has limitations. First, we included a small amount of image data. This impacts the generalizability of our findings. However, this report primarily aims to describe the implementation of DL-reconstruction in clinical routine rather than to systematically and comprehensively evaluate the resulting image quality. For image quality assessment, body region focused clinical studies are still required. A further limitation is the fact that DL-reconstruction wasn't applied on 3D MR sequences yet. DL-based reconstruction algorithms for 3D sequences are still being developed by our team.

To conclude, DL image reconstruction can be implemented in clinical workflow and enables accelerated image acquisition allowing a remarkable time saving of more than 50% while maintaining excellent image quality for TSE sequences.

Abbreviations

Artificial Intelligence (AI); Convolutional Neural Network (CNN); Compressed Sensing (CS); Deep Learning (DL); Half-fourier Single-shot Turbo spin Echo (HASTE); Image Quality (IQ); Machine Learning (ML); Magnetic Resonance Imaging (MRI); Parallel Imaging (PI); Signal-to-Noise Ratio (SNR); Specific Absorption Rate (SAR); Time of Acquisition (TA); T2-weighted (T2w); Turbo Spin Echo (TSE); Parallel Acquisition Technique (PAT).

Declarations

Ethics approval and consent to participate

Institutional review board approval was obtained for this prospective, monocentric study and informed consent obtained from all participants. All study procedures were conducted in accordance with the ethical standards as laid down in the 1964 Declaration of Helsinki and its later amendments.

The institutional review board of our university (Ethik-Kommission, Prof. Dr. med. Karl Jaschonek, Medizinische Fakultät, Universitätsklinikum Tübingen) approved the study under the committe's reference number: "055/2017B02".

Consent for publication

Written informed consent was obtained from all subjects in this study.

Availability of data and materials

The datasets generated and analyzed during the current study are not publicly available to ensure data privacy protection but are available from the corresponding author on reasonable request.

Competing interests

All authors declare that they have no competing interests.

Funding

Support by an institutional research grant by Siemens AG.

Authors' contributions

Judith Herrmann	Report conception and design. Data acquisition, analysis and interpretation. Drafting and revising the manuscript.
Sebastian Gassenmaier	Report design. Data interpretation. Revising the manuscript.
Thomas Kuestner	Report design. Drafting and revising the manuscript.
Matthias Kuendel	Data acquisition. Revising the manuscript.
Marcel Dominik Nickel	Report design. Data analysis and interpretation. Revising the manuscript.
Gregor Koerzdoerfer	Report conception and design. Revising the manuscript.
Mahmoud Mostapha	Report conception and design. Revising the manuscript.
Mariappan Nadar	Report conception and design. Revising the manuscript.
Ahmed Othman	Report conception and design. Data acquisition, analysis and interpretation. Revising the manuscript.

Acknowledgements

The authors would like to thank Andreas Lingg for his work on the data acquisition.

References

1. Vanderby S, Badea A, Pena Sanchez JN, Kalra N, Babyn P. Variations in Magnetic Resonance Imaging Provision and Processes Among Canadian Academic Centres. Can Assoc Radiol J. 2017;68(1):56–65.

2. Lustig M, Donoho D, Pauly JM. Sparse MRI: The application of compressed sensing for rapid MR imaging. Magn Reson Med. 2007;58(6):1182–95.
3. Deshmane A, Gulani V, Griswold MA, Seiberlich N. Parallel MR imaging. J Magn Reson Imaging. 2012;36(1):55–72.
4. Knoll F, Hammernik K, Zhang C, Moeller S, Pock T, Sodickson DK, et al. Deep-Learning Methods for Parallel Magnetic Resonance Imaging Reconstruction: A Survey of the Current Approaches, Trends, and Issues. Ieee Signal Proc Mag. 2020;37(1):128–40.
5. Lin DJ, Johnson PM, Knoll F, Lui YW. Artificial Intelligence for MR Image Reconstruction: An Overview for Clinicians. Journal of Magnetic Resonance Imaging. 2020.
6. Hyun CM, Kim HP, Lee SM, Lee S, Seo JK. Deep learning for undersampled MRI reconstruction. Phys Med Biol. 2018;63(13).
7. Recht MP, Zbontar J, Sodickson DK, Knoll F, Yakubova N, Sriram A, et al. Using Deep Learning to Accelerate Knee MRI at 3 T: Results of an Interchangeability Study. AJR Am J Roentgenol. 2020:1–9.
8. Knoll F, Hammernik K, Kobler E, Pock T, Recht MP, Sodickson DK. Assessment of the generalization of learned image reconstruction and the potential for transfer learning. Magn Reson Med. 2019;81(1):116–28.
9. Hammernik K, Klatzer T, Kobler E, Recht MP, Sodickson DK, Pock T, et al. Learning a variational network for reconstruction of accelerated MRI data. Magn Reson Med. 2018;79(6):3055–71.
10. Schlemper J, Caballero J, Hajnal JV, Price AN, Rueckert D. A Deep Cascade of Convolutional Neural Networks for Dynamic MR Image Reconstruction. IEEE Trans Med Imaging. 2018;37(2):491–503.
11. Arjovsky M, Chintala S, Bottou L. Wasserstein gan. arXiv preprint arXiv:170107875. 2017.
12. LeCun Y, Bengio Y, Hinton G. Deep learning. Nature. 2015;521(7553):436–44.
13. Aggarwal HK, Mani MP, Jacob M. MoDL: Model-Based Deep Learning Architecture for Inverse Problems. IEEE Trans Med Imaging. 2019;38(2):394–405.
14. Kustner T, Fuin N, Hammernik K, Bustin A, Qi HK, Hajhosseiny R, et al. CINENet: deep learning-based 3D cardiac CINE MRI reconstruction with multi-coil complex-valued 4D spatio-temporal convolutions. Sci Rep-Uk. 2020;10(1).
15. Eo T, Jun Y, Kim T, Jang J, Lee HJ, Hwang D. KIKI-net: cross-domain convolutional neural networks for reconstructing undersampled magnetic resonance images. Magnetic Resonance in Medicine. 2018;80(5):2188–201.
16. Wang SS, Su ZH, Ying L, Peng X, Zhu S, Liang F, et al. Accelerating Magnetic Resonance Imaging Via Deep Learning. I S Biomed Imaging. 2016:514–7.
17. Han Y, Sunwoo L, Ye JC. k-Space Deep Learning for Accelerated MRI. Ieee T Med Imaging. 2020;39(2):377–86.
18. Lee DW, Yoo JJ, Tak SH, Ye JC. Deep Residual Learning for Accelerated MRI Using Magnitude and Phase Networks. Ieee T Bio-Med Eng. 2018;65(9):1985–95.

19. Qin C, Schlemper J, Caballero J, Price AN, Hajnal JV, Rueckert D. Convolutional Recurrent Neural Networks for Dynamic MR Image Reconstruction. Ieee T Med Imaging. 2019;38(1):280–90.
20. Yang G, Yu SM, Dong H, Slabaugh G, Dragotti PL, Ye XJ, et al. DAGAN: Deep De-Aliasing Generative Adversarial Networks for Fast Compressed Sensing MRI Reconstruction. Ieee T Med Imaging. 2018;37(6):1310–21.
21. Mardani M, Gong EH, Cheng JY, Vasanawala SS, Zaharchuk G, Xing L, et al. Deep Generative Adversarial Neural Networks for Compressive Sensing MRI. Ieee T Med Imaging. 2019;38(1):167–79.
22. Zhu B, Liu JZ, Cauley SF, Rosen BR, Rosen MS. Image reconstruction by domain-transform manifold learning. Nature. 2018;555(7697):487-+.
23. Chen F, Taviani V, Malkiel I, Cheng JY, Tamir JI, Shaikh J, et al. Variable-Density Single-Shot Fast Spin-Echo MRI with Deep Learning Reconstruction by Using Variational Networks. Radiology. 2018;289(2):366–73.
24. Sandino CM, Lai P, Vasanawala SS, Cheng JY. Accelerating cardiac cine MRI using a deep learning-based ESPIRiT reconstruction. Magnetic Resonance in Medicine. 2020.
25. Hosseini SAH, Zhang C, Weingartner S, Moeller S, Stuber M, Ugurbil K, et al. Accelerated coronary MRI with sRAKI: A database-free self-consistent neural network k-space reconstruction for arbitrary undersampling. Plos One. 2020;15(2).
26. Fuin N, Bustin A, Kustner T, Oksuz I, Clough J, King AP, et al. A multi-scale variational neural network for accelerating motion-compensated whole-heart 3D coronary MR angiography. Magn Reson Imaging. 2020;70:155–67.

Figures

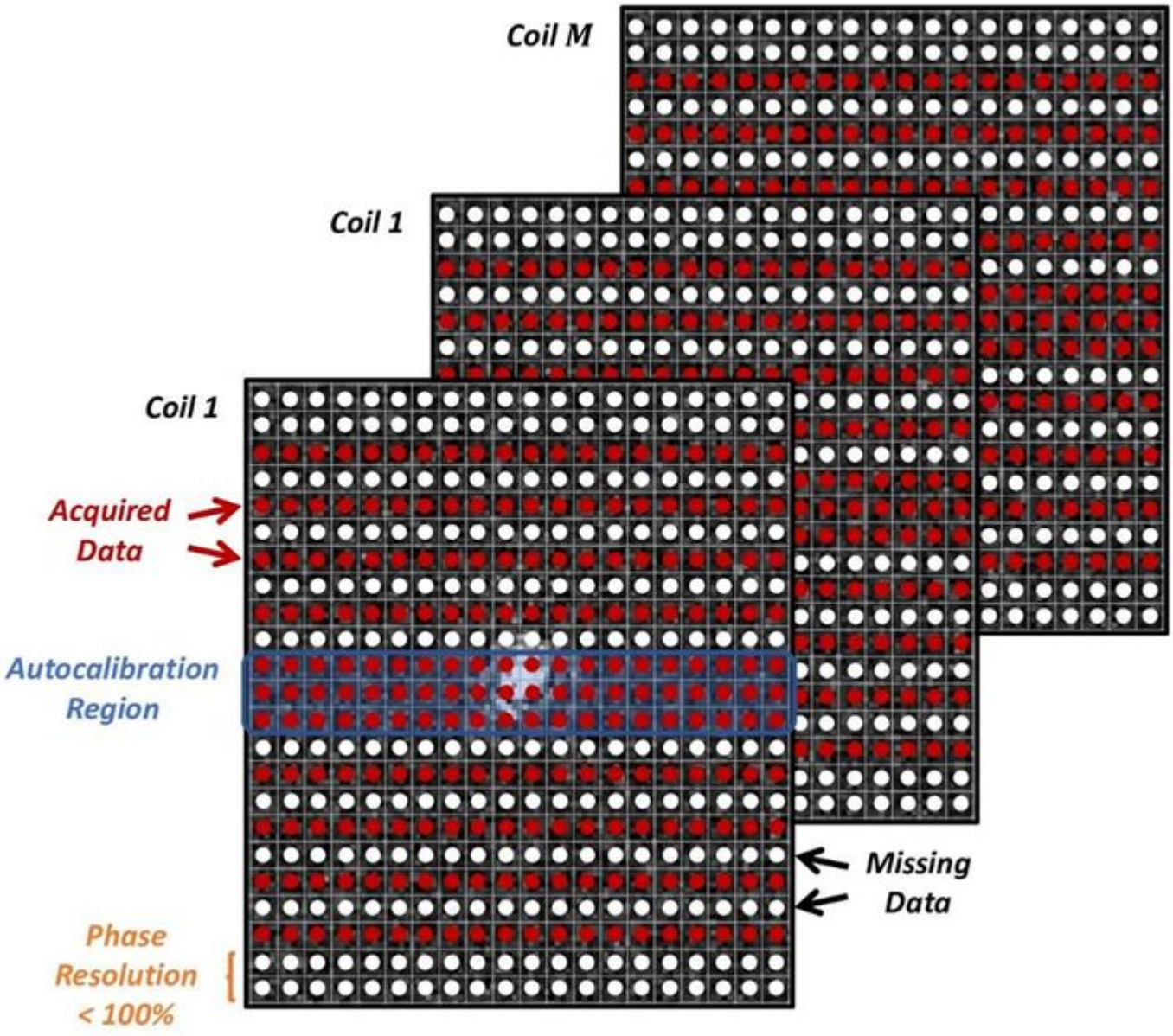

Figure 1

Exemplary sampling pattern used for the k-space data acquisition. Along the phase encoding direction, data are under-sampled by an acceleration factor R. An auto calibration region covering the center of k-space is acquired either along with the imaging acquisition or separately with a different image contrast. A fraction of the periphery may be skipped, usually referred to as phase resolution.

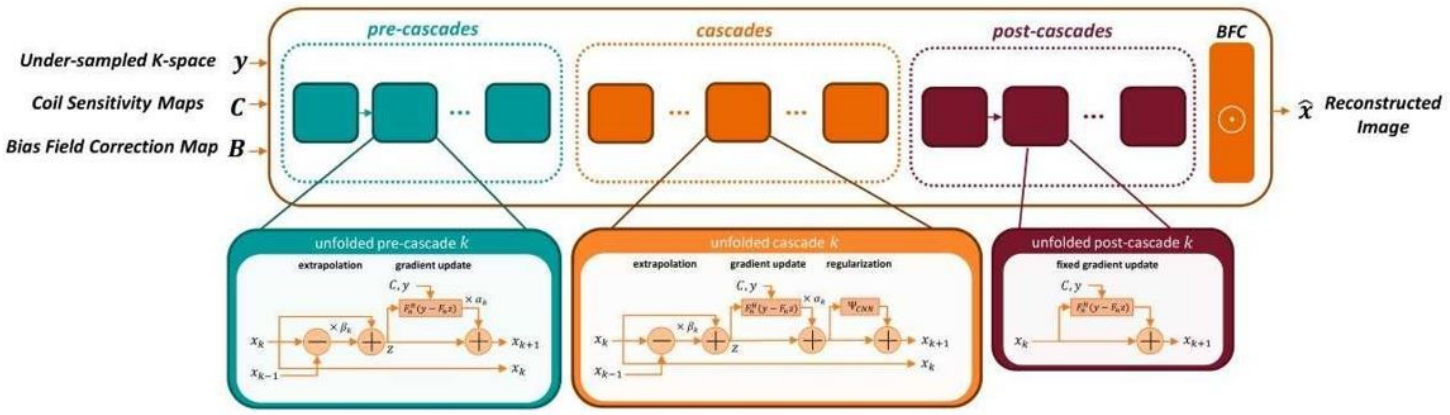

Figure 2

Architecture of the fixed iterative reconstruction scheme. Pre-cascades address data consistency and generate an image similar to conventional parallel imaging, cascades use an alternating scheme between data-consistency and regularization, post-cascades reemphasize consistency of reconstructed image and acquired data. Note that only the regularization is a Convolutional Neural Network (CNN). Nevertheless, the whole architecture can be presented by a general network.

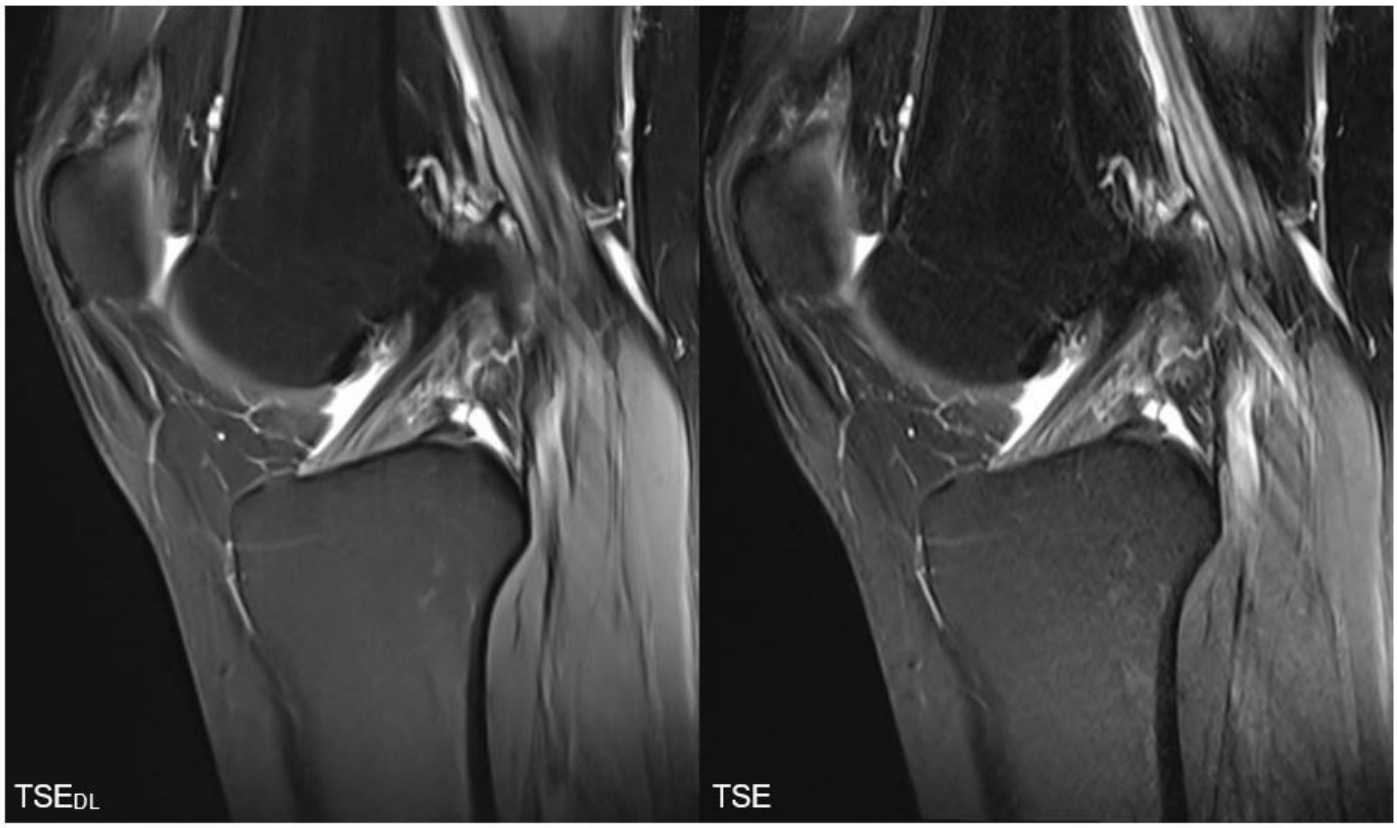

Figure 3

Example of a Deep Learning (left) and standard (right) turbo spin echo image of the knee.

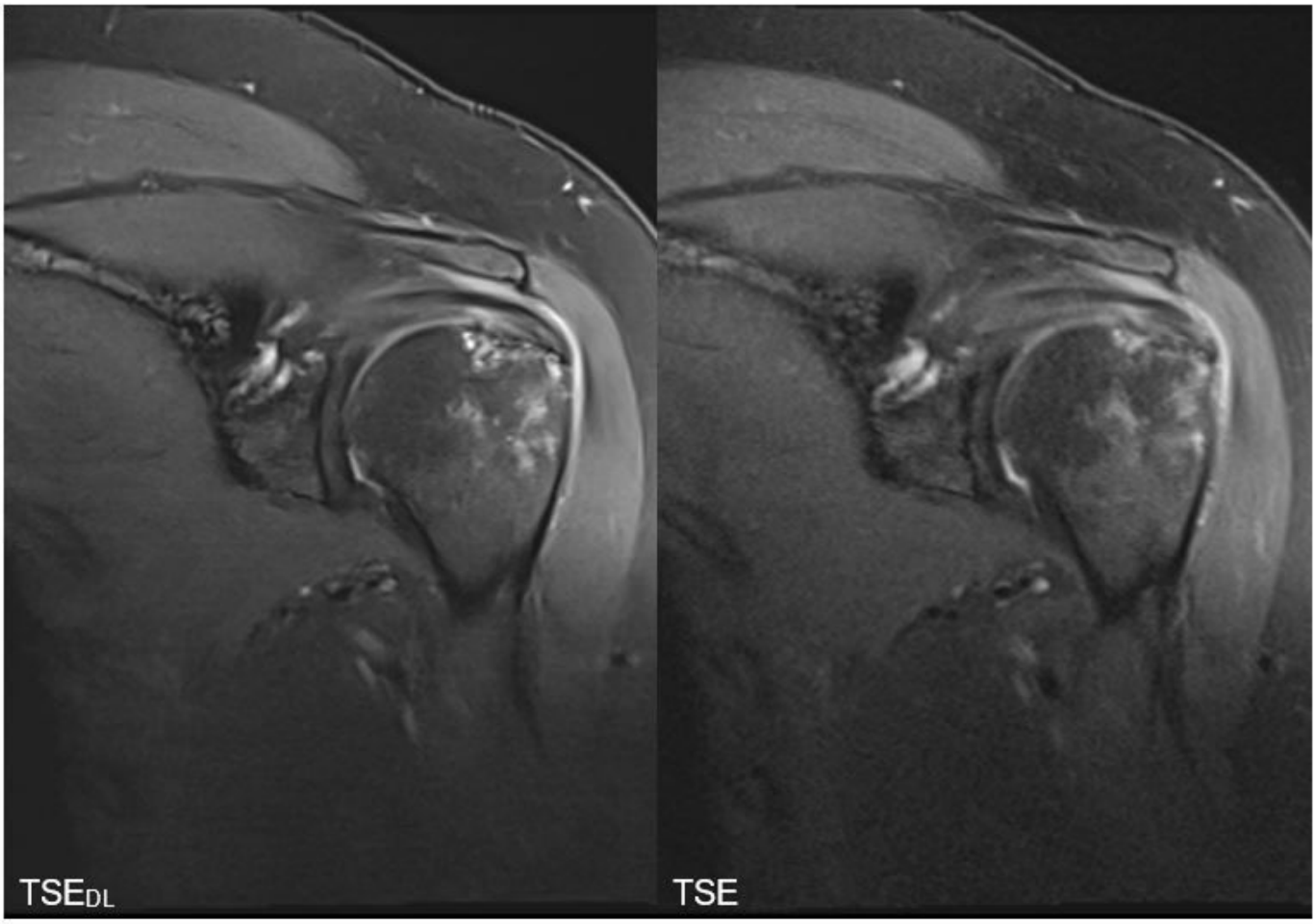

Figure 4

Example of a Deep Learning (left) and standard (right) turbo spin echo image of the shoulder.

Figure 5

Example of a Deep Learning (left) and standard (right) T1- and T2-weighted turbo spin echo image of the lumbar spine.